# Numerical study of a well boat operating at a fish farm in current

Yugao Shen[a,b,*], Marilena Greco[a,b,c], Odd M. Faltinsen[a,b]

[a] *Department of Marine Technology, Norwegian University of Science and Technology (NTNU), Trondheim, NO-7491, Norway*
[b] *Centre for Autonomous Marine Operations and Systems (AMOS), NTNU, Trondheim, NO-7491, Norway*
[c] *CNR-INM, Institute of Marine Engineering, Rome, Italy*

**Abstract**

Dynamic response of a well boat operating at a fish farm in current is investigated numerically. An objective is to determine the operational conditions of the well boat. In terms of the fish farm, a realistic set-up (with single cage) is considered, including a floating collar, an elastic sinker tube, a flexible-closed net cage and a complex mooring system. A time-domain solution is used to find the steady configuration and response. Transverse viscous current loads are estimated using the cross-flow principle. The drag coefficients are obtained empirically by considering cross-sectional details, free surface and three-dimensional (3D) flow effects. The drag force is experimentally validated. The effect of the ship wake on the net loading is also assessed.

The most critical scenario with the well boat placed at the weather side of the fish farm is analyzed in detail. Critical response variables for operational limits are the maximum anchor-line tensions and floater stresses. Numerical results show that the anchor loads will increase more than 40% in small current velocities and up to 90% in high current velocities due to the viscous current loads on the boat. There is also a strong increase of the floating collar deformations and stresses when the well boat is in contact with the floating collar.

A sensitivity analysis has been carried out to identify the physical parameters affecting the anchor loads and the maximum stress in the floating collar. From our studies, the anchor loads are more sensitive to current direction, bottom weight system, sinker tube depth and mooring line properties (pretension load, anchor chain weight, etc.) and less sensitive to other parameters such as floating collar stiffness and cross-sectional drag coefficients of the well boat. The shading effect of the well boat on the fish-farm inflow has been examined and appeared not negligible with 4% to 10% reduction of the anchor loads for the studied current conditions. The maximum stress in the floating collar is sensitive to well-boat loads related parameters (current direction, cross-sectional drag coefficient) and pretension load in the anchor line; not so sensitive to net loading related parameters such as sinker tube depth and sinker tube weight.

Lastly, the operational conditions of the well boat at the fish farm were discussed. Numerical results show that the maximum stresses in the floating collar should be of major concern. The loads in the mooring lines are moderate compared with the corresponding breaking limits.

*Keywords:* Fish farm, Well boat, Current, Critical physical parameters, Operational conditions

*Corresponding author
*Email address:* yugao.shen@ntnu.no (Yugao Shen)

## 1. Introduction

The global shortage of food is becoming increasingly serious due to the rise in world population. More food is expected to come from the ocean, which has a huge potential and increased aquaculture is envisaged. Due to limited available near-shore space and growing impact to the local ecosystem, the expansion of traditional near-shore aquaculture is getting more difficult. So there is a trend of moving marine fish farms to more exposed areas where waves and current are more energetic. This is of concern in terms of probability of structural failure of fish farms. To ensure safe operation, the size of traditional systems is expected to increase and use of novel fish-farm designs is explored. A traditional floating collar fish farm system typically comprises a floating collar, a flexible net cage, a sinker tube, moored with a complex mooring system. In order to guarantee the robustness of the fish farm system, we need to have a reliable prediction of hydrodynamic forces and motions of the different components during the early design stage.

Apart from the challenge from the fish farm perspective, operating fish farms in exposed areas will also increase the probability of routine well boat operations in severe weather conditions. A well boat is a fishing vessel with a well or tank for the storage and transport of live fish. A typical well boat operation can be categorized into three phases: approaching, loading/offloading and leaving. During the loading/offloading phase, the well boat is moored directly to the fish farm, which may significantly increase the mooring loads and the floating collar deformations and thus endanger the structural integrity of the fish farm. So there is a need to have a detailed investigation of the influence of the well boat on the fish farm and identify the operational conditions for performing such load/offloading operation.

Many investigations have been done for the fish farm system. For example, Dong et al. (2010a) and Li et al. (2016) studied experimentally and theoretically the vertical responses of an isolated elastic-circular, moored floater in regular waves. Lader and Fredheim (2006) applied a truss model to investigate the dynamic properties of a two-dimensional flexible net sheet exposed to waves and current. Zhan et al. (2006) performed an analytical and experimental investigation of drag forces on a planar net panel in current. Model tests with similar set-up in waves were conducted by Lader et al. (2007). A two-dimensional numerical and experimental study of a floater with net and sinker tube in waves and current was performed by Bardestani and Faltinsen (2013). Circular aquaculture net cages in waves and current were investigated by many researchers, for instance, Huang et al. (2006, 2008), Zhao et al. (2007), Kristiansen and Faltinsen (2012, 2015) and Xu et al. (2013). Hydrodynamic behavior of gravity cage in irregular waves was also studied by Dong et al. (2010b), Xu et al. (2011) and Li et al. (2013). He et al. (2015) studied experimentally the influence of fish in a net cage on the mooring loads in waves and current. They showed that if the fish touched the netting in current, there was more than 10% increase in the mooring loads. High waves caused the fish to go to the bottom of the net cage and increase the mooring loads. Recently, Shen et al. (2018b) presented a comparison of numerical calculations with model test measurements of mooring loads for a marine fish farm in both regular and irregular waves. A realistic fish cage featuring all the main components presented in a full-scale sea cage system was considered in their study. Faltinsen and Shen (2018) presented a review on hydrodynamic and structural aspects of fish farms. The behavior of traditional type fish farms with net cages and closed fish farms in waves and current were discussed. Numerical results on the stochastic behavior of bending stresses in the floater of a realistic net cage in extreme wave conditions were also presented. More references

to relevant works can be found in the mentioned papers. In reality, many cages operate in close proximity, which affect the current and wave loads. Future studies are needed.

Little research has been done for the scenario when a well boat operates at the fish farm. In particular, to the authors' knowledge no experimental study has been carried out so far. Shen et al. (2016) performed a preliminary numerical study of a coupled well boat-fish farm system in waves and current. A simplified fish farm system was considered with an elastic torus, a flexible-circular-bottomless net cage, sink weights and a complex mooring system. They showed that the mean steady-state anchor loads for the coupled system increase significantly compared with those for the fish farm system alone due to the nonlinear viscous forces and mean wave drift loads on the boat. The presence of the boat will also exert an important influence on the floating collar motions. They demonstrated that the influence of the well boat on the fish farm was not negligible. The effect of the well boat is seldom considered in the design of fish farms and more research is needed. In the present paper, we continue the study by Shen et al. (2016) and perform a more detailed analysis of a more realistic coupled wellboat-fish farm system in current. The influence of fish present in the net cage is neglected. Sea conditions used in the analysis are according to the environmental classification given by Norwegian standard NS9415:2009, see Table 1. Only the classification for current will be used in the present study. Numerical results of the coupled system exposed to irregular waves and current are investigated by Shen et al. (2018a).

Table 1: Environmental classification given in terms of significant wave height $H_s$, peak period $T_p$ and current velocity $U_\infty$ according to NS9415 (2009).

| **Wave** | $H_s$(m) | $T_p$(s) | **Exposure** | **Current** | $U_\infty$(m/s) | **Exposure** |
|---|---|---|---|---|---|---|
| A | 0.0 - 0.5 | 0.0 - 2.0 | Small | a | 0.0 - 0.3 | Small |
| B | 0.5 - 1.0 | 1.6 - 3.2 | Moderate | b | 0.3 - 0.5 | Moderate |
| C | 1.0 - 2.0 | 2.5 - 5.1 | Heavy | c | 0.5 - 1.0 | Heavy |
| D | 2.0 - 3.0 | 4.0 - 6.7 | High | d | 1.0 - 1.5 | High |
| E | >3.0 | 5.3 - 18.0 | Extreme | e | >1.5 | Extreme |

A modern design well boat and a realistic fish farm are considered in the analysis. The fish-farm dimensions are those for systems used nowadays in protected areas, which means that we examine their behavior if moved to more exposed regions. The modeling of the fish farm was introduced and validated by Shen et al. (2018b). The motions of the well boat and wave drift forces are solved by the classical seakeeping theory. In the present paper, the transverse viscous current loads on the well boat are considered based on the cross-flow principle documented in Faltinsen (1990) and an empirical method is proposed to estimate the cross-sectional drag coefficients. A detailed sensitivity analysis is also performed by examining the influence of different parameters used in the modeling of mooring loads. Then, operational conditions of the well boat at the fish farm are discussed and important parameters in this context are identified. Operational conditions denote the weather window suitable for performing such loading/offloading operation and are determined based on the criteria that the structural integrity of the fish farm is not endangered by the boat.

The paper is organized as follows. First, a description of the numerical set-up of the coupled well boat-fish farm system is given in section 2. Then, numerical modelings of the fish-farm system and the well boat

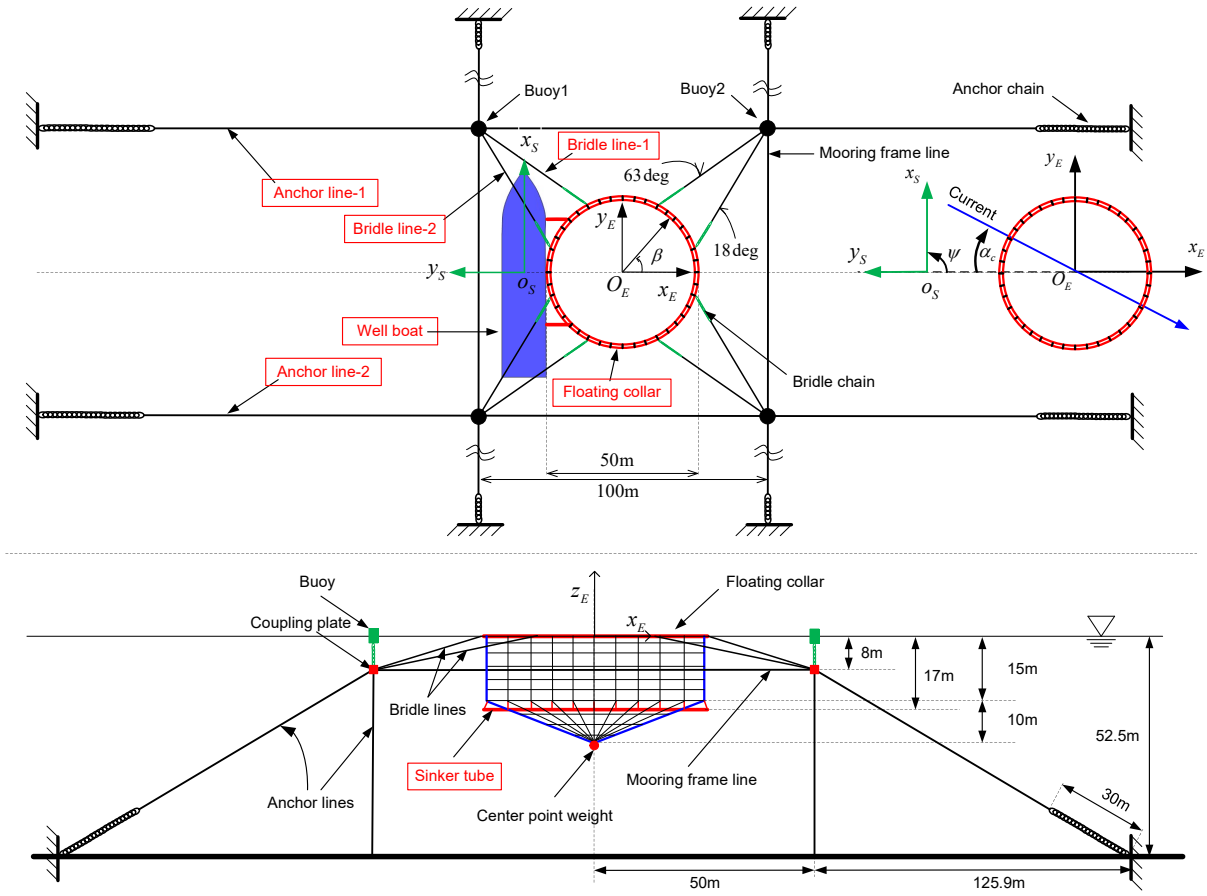


Figure 1: Configurations of the coupled well boat-fish farm system with definitions of different coordinate systems. Upper: top view. The floating collar is duplicated in the right part of the sketch to define current direction $\alpha_c$ and boat heading angle $\psi$. Lower: side view.

are briefly introduced in section 3. The strategy used for their coupling is also explained. Lastly, numerical response of the coupled system in current is presented in section 4. Special attention is paid to the load in one of the front anchor lines and the bending stresses in the floating collar. A detailed sensitivity analysis is also performed and the effects of different parameters on the anchor loads and the maximum bending stresses are discussed. Finally, the operational conditions of the well boat during the loading/offloading operation are determined.

## 2. Numerical set-up

The main arrangement and dimensions of the coupled fish farm-well boat system are described in this section. For the fish farm, similar set-up used by Shen et al. (2018b) is adopted in the present study, including two concentric floating tubes, an elastic sinker tube, a cylindrical net cage with a conical bottom, a mooring system comprising bridle lines, mooring frame lines, mooring buoys, coupling plates, chains connecting the coupling plates to the buoys and the anchor lines attaching the system to the sea bed, see Figure 1. The parameters and dimensions of different components are given in Tables 2 and 3. Some of the parameters are different from those given by Shen et al. (2018b), to represent more realistic values. The parameters shown

Table 2: Parameters of the floating collar, net cage and sinker tube. The position of the center point weight $W_c$ is shown in Figure 1.

| Description | Symbol | Value | Unit |
|---|---|---|---|
| **Floating collar** | | | |
| Number of tubes | - | 2 | - |
| Diameter inner ring | $D_{f1}$ | 50 | m |
| Diameter outer ring | $D_{f2}$ | 51.8 | m |
| Tube section diameter | $d_f$ | 450 | mm |
| Tube bending stiffness | $EI_f$ | $7.72 \times 10^5$ | $\mathrm{Nm}^2$ |
| Tube mass | $m_f$ | 32.54 | kg/m |
| **Net cage** | | | |
| Diameter | $D_c$ | 50 | m |
| Depth of vertical net | $h_u$ | 15 | m |
| Depth of cone net | $h_l$ | 10 | m |
| Net twine diameter | $d_w$ | 2.7 | mm |
| Net mesh-bar length | $l_w$ | 19.3 | mm |
| Net E-module | $E_{\mathrm{net}}$ | $8 \times 10^8$ | $N/m^2$ |
| Net solidity ratio | Sn | 0.26 | - |
| Center point weight | $W_c$ | 200 | kg |
| **Sinker tube** | | | |
| Tube diameter | $D_s$ | 51.8 | m |
| Tube section diameter | $d_s$ | 280 | mm |
| Tube depth | $h_s$ | 17 | m |
| Tube bending stiffness | $EI_s$ | $2.0 \times 10^5$ | $\mathrm{Nm}^2$ |
| Sectional mass in water | $w_s$ | 50 | kg/m |

in Shen et al. (2018b) were derived based on the experimental data from Nygaard (2013). Since 'ordinary' ropes were used in the experiments, the corresponding full-scale stiffness of the bridle lines and frame lines are larger than those used in commercial full-scale cages. So instead, we use realistic full-scale values in the present study. Also, the stiffness of the front two anchor lines was about 110 kN/m in Nygaard (2013), as was a specified value in the experiments, while in the present case the corresponding value is about 55 kN/m, based on the realistic length, diameter and Young's module given for the anchor lines.

For the well boat, a modern design well boat from Rolls-Royce Marine, is used in the study. The three-dimensional (3D) numerical panel model used in the potential-flow calculations together with the body plan are shown in Figure 2. The principal dimensions are given in Table 4.

Two different inertial and Earth-fixed coordinate systems are used in the simulations and are defined in Figure 1. One is the Cartesian right-handed coordinate system $O_E x_E y_E z_E$ with the vertical $z_E$-axis positive upwards through the center of the floating collar in calm water. The other is the seakeeping coordinate system $O_S x_S y_S z_S$ with origin in the undisturbed free surface $z_E$=0. The vertical $z_S$-axis is positive upwards through the center of gravity of the boat in the mean-ship configuration and the horizontal $x_S$-axis points towards the bow. The current direction $\alpha_c$ is defined in the figure and $\alpha_c = 0^{\mathrm{o}}$ means that the current

Table 3: Parameters of the mooring system. All ropes are almost without weight in water. All ropes Young's module $E_{\text{rope}}$=1.8 GPa and the chain Young's module $E_{\text{chain}}$=105 GPa. Positions where the two bridle lines are attached to the floating collar are defined in the coordinate system $O_E x_E y_E z_E$.

| **Description** | **Value** | **Unit** |
|---|---|---|
| **Bridle lines** | | |
| Position (bridle-1) | 117 | degrees |
| Position (bridle-2) | 162 | degrees |
| Rope diameter | 48 | mm |
| Rope length | 44.2 | m |
| Chain diameter | 19 | mm |
| Chain length | 5.47 | m |
| Chain mass | 8.66 | kg/m |
| Bridle line stiffness | 72.7 | kN/m |
| **Anchor lines** | | |
| Line length | 133.5 | m |
| Rope length | 103.5 | m |
| Rope diameter | 64 | mm |
| Chain length | 30 | m |
| Chain diameter | 36 | mm |
| Chain mass | 28.73 | kg/m |
| Anchor line stiffness | 55.1 | kN/m |

| **Description** | **Value** | **Unit** |
|---|---|---|
| **Frame lines** | | |
| Length | 100 | m |
| Depth | 8 | m |
| Diameter | 64 | mm |
| Frame line stiffness | 57.9 | kN/m |
| **Buoys system** | | |
| Number of buoys | 4 | - |
| Buoy diameter | 1.55 | m |
| Buoy length | 2.34 | m |
| Buoy mass | 146.9 | kg |
| Chain diameter | 19 | mm |
| Chain length | 7 | m |
| Chain mass | 8.66 | kg/m |
| Coupling plate mass | 55 | kg |

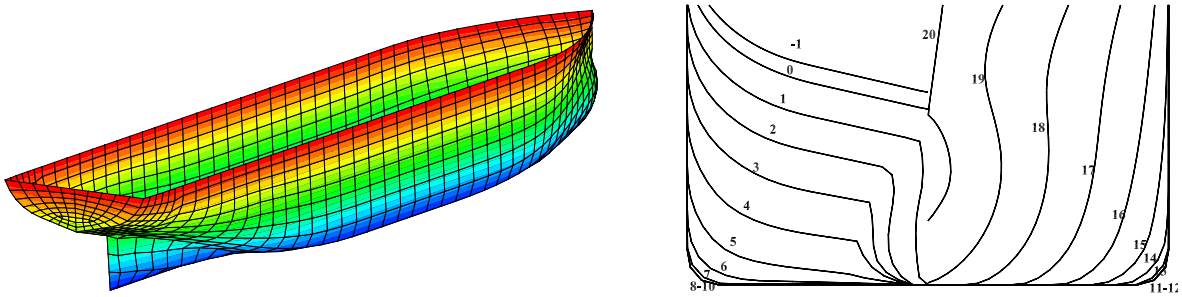


Figure 2: Submerged geometry of the well boat. Left: panel model. Right: body plan. Numbering of sections is also given with section 1 in the aft part of the boat.

direction coincides with the positive $x_E$ direction. The heading angle of the boat $\psi$ is also defined in Figure 1 and $\psi = 0^{\text{o}}$ means that the bow of the boat points towards the positive $x_E$-axis.

The well boat can be moored in different positions relative to the fish farm. No thruster action is considered, which is common practice in order to avoid possible net suction. Assuming a scenario with main inflow direction along positive $x_E$, three relevant well-boat set-ups are given in Figure 3. Set-up A: at the weather side of the floating collar; set-up B: at the leeward side; set-up C: between cages of a multi-cage fish-farm system with bow against the inflow. Each set-up has pros and cons. It will be difficult for the boat to detach from the fish farm with set-up A in severe sea conditions and this set-up is expected to be the most critical in terms of mooring loads and floating collar stresses. On localities with strong current, the

well boat should avoid connecting to the fish farm with set-up B as there is a risk of the net drifting into the propeller. The system with set-up C can significantly reduce the external loads from the boat and therefore is not so critical. In the present paper, we will mainly investigate the coupled system with set-up A, and the results for the system with the other two set-ups will be just briefly discussed.

Table 4: Principal dimensions of the well boat.

| | |
|---|---|
| Length between perpendiculars ($L$) | 70 m |
| Breadth ($B$) | 15 m |
| Draft ($D$) | 6.7 m |
| Displacement volume ($\nabla$) | 5145 $m^3$ |
| Block coefficient ($C_b$) | 0.75 |
| Mid-ship coefficient ($C_m$) | 0.99 |
| Height of center of gravity ($KG$) | $0.75D$ |
| $OG = KG - D$ | $-0.25D$ |
| Roll gyration radius | $0.35B$ |
| Pitch gyration radius | $0.28L$ |
| Yaw gyration radius | $0.28L$ |
| Transverse metacentric height (GM) | 1.6 m |
| Bilge-keel length ($l_{bk}$) | $0.3L$ |
| Bilge-keel breadth ($b_{bk}$) | $0.02B$ |

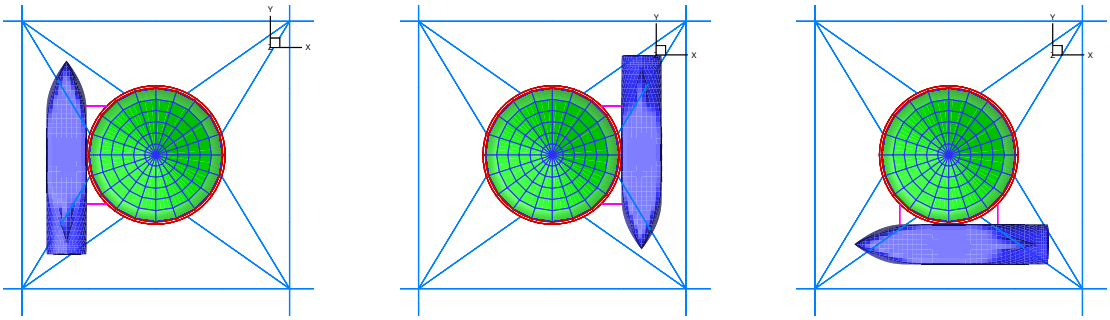

Figure 3: Different set-ups with the well boat moored to the fish farm. The incident current is in the $x$-direction. Left: set-up A, heading angle of the boat $\psi = 90^o$ (weather side). Middle: set-up B, $\psi = 270^o$ (leeward side). Right: set-up C, $\psi = 180^o$ (bow against current).

## 3. Theoretical and numerical model

In this section, the modeling of the coupled well boat-fish farm system is presented. A time-domain solution is used to find the steady configuration and response. First, the modeling of well boat loads is given. An empirical way to estimate the cross-sectional drag coefficients of the well boat in current is proposed. Then the modeling of different fish-farm components is briefly illustrated. Finally, the strategy used for the well boat-fish farm coupling is explained and the method to measure the contact force between them is addressed.

### 3.1. The well boat

The transient motions of the well boat are solved in the seakeeping coordinate system $O_S x_S y_S z_S$. Transient linear potential-flow effects as proposed by Cummins (1962) are included in the equations of motion. The transient motions will decay after a short time in the simulations when only viscous current loads are considered. Due to coupling with the fish farm, apart from the current loads, the right-hand side of the equations of motion will also have other external loads with respect to those of a single ship. These may include contact forces and connection-line forces. In the following we will mainly pay attention to the estimation of steady-state viscous current loads, the estimations of the others are given in section 3.3.

The boat interaction with a current, with generic direction relative to the boat, will lead to viscous loads. In principle, these loads can be affected by the presence and coupling with the fish farm, but this can be neglected as a first approximation. Under these assumptions, to estimate the current loads on the boat, dedicated model tests or Computational Fluid Dynamics (CFD) simulations could be used. The former involve a cost and will have the issue of Reynolds number scaling; the latter become more and more popular because less costly but require suitable validation and can be time-consuming for performing converged simulations at high Reynolds numbers. An argument against CFD is also that the well boat is a subsystem and numerical tools for the different subsystems must be balanced in complexity. The many meshes of the netting of a fish cage prohibits CFD and complete structural modelling. For a more efficient and still physically-sound estimation of current loads, here we follow the procedure documented by Faltinsen (1990). We assume that the current loads can be decomposed in transverse and longitudinal loads caused, respectively, by the transverse and by the longitudinal component of the current velocity with respect to the ship main axis. The transverse loads are mainly connected with flow separation along the vessel as long as the angle between the current direction and the longitudinal ship direction is not small and can be estimated with the cross-flow principle. They lead in general to a 3D transverse force and to a yaw moment. In addition a potential-flow Munk yaw moment is also caused by the current. The longitudinal force is mainly connected with frictional stresses. In particular, the 3D transverse ($Y_{CF}$) and longitudinal ($X_{CF}$) forces can be written as

$$\begin{aligned} Y_{CF} &= -0.5\rho \int_L \left[C_D\left(x\right) V_{CF} \left|V_{CF}\right| D\left(x\right)\right] dx \\ X_{CF} &= -0.5\rho C_F U_{CF} \left|U_{CF}\right| S \end{aligned} \tag{1}$$

Here $\rho$ is the water density, $C_D(x)$ is the drag coefficient for cross-flow past an infinitely long cylinder with the cross-sectional area of the ship at the longitudinal coordinate $x$, modified by 3D effects due to flow separation around the ship ends. $V_{CF}$ is the transverse current component and $D(x)$ is the sectional draft. Similarly, $C_F$ is the frictional coefficient, $U_{CF}$ is the longitudinal current component and $S$ is the wetted surface area of the ship hull. $V_{CF} = U_\infty \sin\beta_c$ and $U_{CF} = U_\infty \cos\beta_c$ with $\beta_c$ the angle between the current velocity $U_\infty$ and the positive longitudinal $x_S$-axis. It means that empirical load coefficients, $C_D$ and $C_F$, are needed and they are estimated using available data from the literature. Information on the applicability and limits of this decomposition approach and cross-flow principle can be found e.g. in Faltinsen (1990).

#### 3.1.1. Transverse viscous force

Within the cross-flow principle, the 2D transverse viscous current force is a drag force. In order to have a reliable prediction of it, we need a reliable estimation of the drag coefficient at the different ship cross-

sections. Faltinsen (1990) showed that cross-flow drag coefficient for ship cross-sections is mainly influenced by the section geometry (beam-to-draft ratio, bilge radius, bilge keel presence and dimensions), Reynolds number, free-surface and three-dimensional (3D) effects. We will briefly explain the different parameters in the present context.

*Flow regimes:* If the cross-section has no sharp corners, the value of the cross-sectional drag coefficient depends on the flow regime in the boundary layer upstream of flow separation (depending on the Reynolds number and surface roughness), i.e. laminar or turbulent boundary layer flow. The two flow regimes are associated with different locations of the flow separation points, so the corresponding drag coefficient will be different (Aarsnes et al., 1985).

*Three-dimensional (3D) effects:* The 3D effects due to the flow around the ship ends tend to reduce the total drag force compared with pure strip theory approach because they tend to reduce locally the inflow velocity at the cross-sections towards the ship ends (Aarsnes et al., 1985).

*Free surface:* The free surface has a significant influence on the drag coefficient and can be approximated as an infinitely long splitter plate, as long as the boundary layer effect due to the splitter plate is negligible. It will change the flow pattern behind the body and cause a reduction of the drag coefficient. More detailed explanation is given by Faltinsen (1990, 2005).

*Cross-sectional shape:* The effect of the cross-sectional shape upon the drag coefficient for typical midship sections is mainly due to the bilge radius $r$, beam-to-draft ratio $B/D$ and bilge keels. An increase in bilge radius will lead to a reduction of the drag coefficient. The beam-to-draft ratio will have influence, but only when $B/(2D) < 0.8$. The presence of the bilge-keels will make the drag coefficient less scale dependent when transforming model values to full scale (Faltinsen, 1990, 2005). The reason is that the flow separation points are at the bilge keels and not determined by the boundary layer flow. Where the flow separation points will significantly influence the drag coefficients.

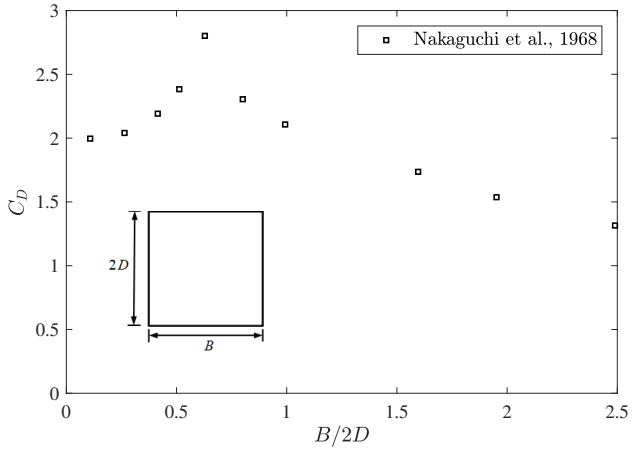


Figure 4: Drag coefficient $C_D$ as a function of aspect ratio $B/(2D)$ for a rectangular two-dimensional cylinder with sharp corners in steady incident flow parallel to the rectangular side with length $B$ (Nakaguchi et al., 1968). Reynolds number Re$= 2U_\infty D/\nu = 2 \sim 6 \times 10^4$ with $U_\infty$ the inflow velocity and $\nu$ the kinematic viscosity.

The next step is to account for the influences of all the above mentioned parameters and give an estimation of the drag coefficient for the different cross-sections. In terms of the flow regime, the cross-flow for different cross-sections of a full-scale well boat should be turbulent, so drag coefficients for turbulent flow should be

adopted. We start with the midship section (section 10). For this, the aspect ratio $B/(2D)$=1.12. According to the experimental data from Nakaguchi et al. (1968), see Figure 4, the drag coefficient $C_D$ for a rectangular section with $B/(2D)$=1.12 and bilge radius $r$=0 in infinite fluid is about 2.0. Faltinsen (1990) documented that the drag coefficient depends strongly on the bilge radius. As $r$ increases, the drag coefficient decreases because the vortex shedding becomes less intense and the dependency can be written as $C_D = C_1 e^{-kr/D} + C_2$, where $C_1$ and $C_2$ are constants of similar magnitude. By fitting the experimental data from Delany (1953), Faltinsen (1990) showed that $k$ may be 6 and $C_D = 0.8e^{-6r/D} + 1.2$ for the case with $B/(2D)$=1. As similar $B/(2D)$ is considered for our midship section, the same $C_D$ expression is assumed. For the midship section, $r/D$= 0.149, then the drag coefficient $C_D$= 1.53.

The free surface will reduce the drag coefficient. In order to have an idea of this reduction effect, we examined the drag coefficients for different cross-section geometries with and without free surface (or splitter plate behind) effect, using data available from the literature. Blevins (1984) showed that the drag coefficient for a sharp-edged square section reduces from 2.0 to 1.45 (Reynolds number = $5 \times 10^4$) due to a splitter plate behind the section, with about 27.5% reduction. The length of the splitter plate was equal to $20D$ and can be roughly seen as infinitely long. Similarly, the drag coefficient for cross-flow past a thin flat plate reduces from 1.9 to 1.38 due to a splitter plate behind, with about 27.3% reduction. The drag coefficient for a circular section with infinity long splitter plate in the middle changes from 1.1 to 0.8 (Reynolds number = $10^4$), with about 27.3% reduction. It is interesting to see that the free surface exerts similar influence on the drag coefficient for different cross-sectional shapes. In the present study, we assume the free surface will reduce the drag coefficient of the midship section by 27.3%, then the drag coefficient for the midship section will be $C_D = 1.11$. The same procedure is applied to estimate the drag coefficient for the midship section of the hull presented in Aarsnes et al. (1985) and nice agreement was achieved with their numerically predicted value.

In the above analysis, the influence of bilge keels is not considered, which may have a big influence. According to the experimental results from Mercier and Huijs (2005), the lateral drag coefficient increases from 0.6 to $0.9 \sim 1.0$ when bilge keels are included. This means that the bilge keels increase the lateral drag coefficient by at least 50%. A simple explanation of the influence of bilge keels is that the flow will be forced to separate at the sharp corner of the bilge keel, which makes the flow field around the corner resembles that for a sharp-edged rectangular section, as shown in Figure 5. So for the midship section with bilge keel, the drag coefficient for a rectangular section with $r$=0 is proposed, which means using $C_D = 2$ instead of $C_D = 1.53$ as basic drag coefficient. Here we neglect the influence of the bilge keel breadth. Considering the free surface effect, the drag coefficient for the midship section becomes $C_D = 2 - 2 \cdot 0.273 = 1.45$. The bilge keels exist from section 7 to section 13, so for simplicity drag coefficient $C_D = 1.45$ is used for all these cross-sections.

For the other ship sections, with geometry close to rectangular, the same procedure introduced above has been followed. The well boat sections near the ship ends present shapes not studied experimentally or numerically. A rough estimation of their drag coefficients has been obtained by interpolating the drag coefficients of ship sections with closest geometries studied numerically in the turbulent-flow regime by Aarsnes et al. (1985). This is an error source but has a limited influence on the average drag coefficient

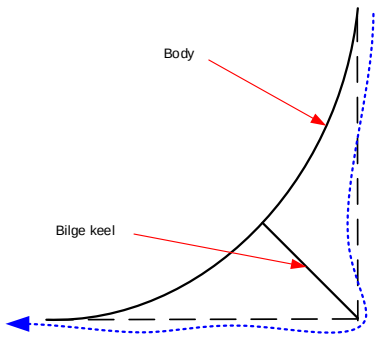


Figure 5: Sketch for flow around the cross-section with bilge keel. Dotted line: sketch of the flow streamline.

for the well boat, as discussed below in the text. The 2D drag coefficient for different sections needs to be lowered as consequence of 3D effects. Since no other study on 3D effects is available, but for the one by Aarsnes et al. (1985), the 3D reduction factor for the cross-section drag coefficient from such research work has been adopted here. The drag coefficients for different sections with and without considering the 3D reduction factor are shown in the left plot of Figure 6. The average drag coefficient with and without considering the reduction effect are 0.9 and 1.06, respectively. The obtained ship average $C_D$ is reasonable compared with that shown in Mercier and Huijs (2005) for a tanker-based FPSO with bilge keels. From our results, the average drag coefficient for the well boat is not much sensitive to the specific value of the drag coefficients for cross-sections close to the ship ends, which are those potentially more connected with estimate errors. In fact, a change in these $C_D$ of 10% would cause a change of about 3% for the average well-boat drag coefficient. In order to assess the method introduced, we applied the same procedure to estimate the transverse drag coefficient for a tanker (without bilge keels) presented by Faltinsen et al. (1979) in loaded condition with their experimental data. The results are shown in the right plot of Figure 6. The empirically estimated average drag coefficient ($C_D = 0.69$) agrees well with that from the model tests ($C_D = 0.68$). This suggests a fair reliability of the followed approach for the $C_D$ prediction. The considered scenarios have minor influence of viscous current yaw moment and will therefore not be detailed discussed.

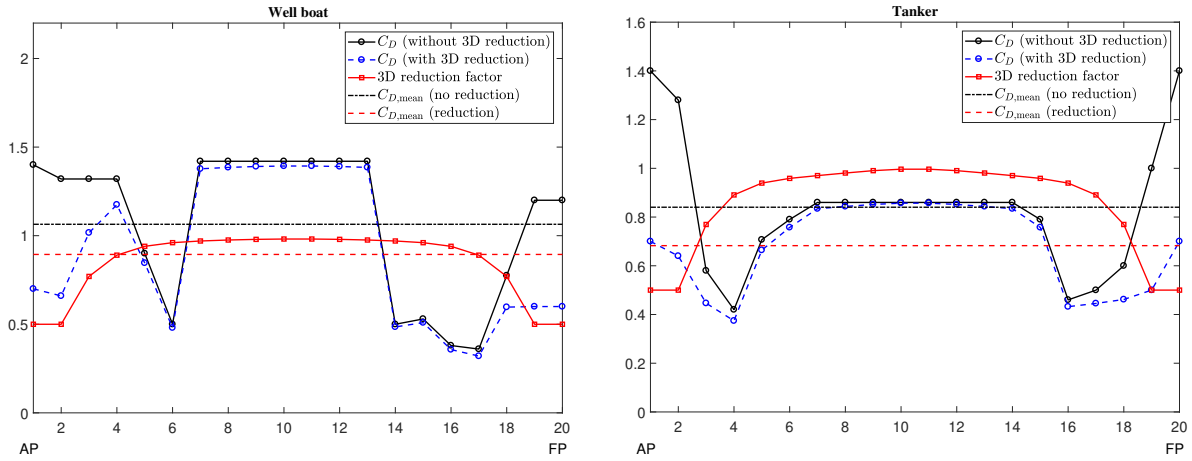


Figure 6: Sectional transverse drag coefficient $C_D$ for different sections of the present well boat (left) and of the tanker documented by Faltinsen et al. (1979). The 2D drag coefficients with and without the 3D reduction effects are shown. The corresponding average drag coefficients are also given.

#### 3.1.2. Longitudinal viscous force

The viscous force in longitudinal direction is mainly due to the friction force on the wetted ship hull. The frictional coefficient $C_F$ is estimated according to the ITTC'57 guidelines as the value for a smooth flat plate in turbulent flow conditions. Pressure drag and roughness effects are not considered as first approximation. Detailed expression can be found in Faltinsen (1990).

### 3.2. Fish farm system

Here we will just outline the numerical models for different components of the fish farm system. More detailed explanation can be found in Shen et al. (2018b).

#### 3.2.1. The net cage

For the structural part, the truss model originally presented by Marichal (2003) and further used by Kristiansen and Faltinsen (2012, 2015), is adopted to describe the net structure. An essential feature in finding the steady net configuration and response is that a time-domain solution is employed instead of an iterative procedure. The steady net configuration in current can differ substantially from the net configuration in calm water. The mesh wires of the net cage are modeled as linear elastic trusses. In terms of the hydrodynamic part, the screen type force model proposed by Kristiansen and Faltinsen (2012, 2015) is used to estimate the hydrodynamic, viscous force acting on the net cage. The model divides the net cage into a number of flat net panels. The force components on a panel are functions of the solidity ratio, the inflow angle and the Reynolds number. The relevant Reynolds number is that based on the physical twine diameter. The screen model accounts implicitly for shadow effects due to the twines, which will not be the case when Morison's equation is applied to each twine. The flow inside the cage will be reduced due to the front part netting without the ship and the reduction coefficient is estimated according to Løland (1991).

#### 3.2.2. The floating collar

The motions of the floating collar with two concentric tubes are solved by generalizing the method proposed by Li et al. (2016) for predicting the motion of an isolated-elastic floating torus, based on a generalized Euler-Bernoulli beam equation that accounts for axial tension and curvature effects. Linear hydrodynamic potential flow of incompressible water is assumed. The same structural model was adopted by Shen et al. (2018b), where the current and incident waves were assumed to be along the positive $x_E$-axis and consequently only structural Fourier modes symmetric about the $x_E$-axis were excited. In the present study, the same current direction is considered in the nominal simulations, however due to the external loads from the well boat, both symmetric and asymmetric modes of the floating collar can be excited. In the $O_E x_E y_E z_E$ reference frame, the motions of the floating collar, $(x_f, y_f, z_f)$, can be expressed by the following Fourier series:

$$x_f(\beta,t) = c_1(t) + v_f(\beta,t)\cos\beta, \quad y_f(\beta,t) = d_1(t) + v_f(\beta,t)\sin\beta, \quad z_f(\beta,t) = a_0(t) + w_f(\beta,t) \tag{2}$$

at time $t$ and location identified by the radial angle $\beta$ along the tube, with $\beta$=0° corresponding to the $x_E$-axis, as defined in Figure 1. Here, the coefficients $c_1$, $d_1$ and $a_0$ represent surge, sway and heave rigid

motions, while

$$w_f(\beta,t) = \sum_{n=1}^{\infty}[a_n(t)\cos(n\beta) + b_n(t)\sin(n\beta)]$$
$$v_f(\beta,t) = \sum_{n=2}^{\infty}[c_n(t)\cos(n\beta) + d_n(t)\sin(n\beta)] \tag{3}$$

are the local vertical (not including heave) and the lateral (radial) elastic deformations, respectively. The terms $a_n\cos(n\beta)$ and $b_n\sin(n\beta)$ denote the vertical modes that are symmetric and anti-symmetric about the $x_E$-axis, respectively. $a_1\cos\beta$ and $b_1\sin\beta$ are the vertical motion due to pitch and roll, respectively. $a_n\cos n\beta$ and $b_n\sin n\beta$, with $n \geq 2$, are purely vertical elastic modes. The coefficients $c_n$ and $d_n$ $(n \geq 2)$ are connected with the horizontal elastic radial mode $n$. By inserting eq.(2) into the curved beam equations with additional tension, multiplying with each Fourier mode and integrating along the floater, we can have the motion equations for different modes. Detailed formulas are omitted here, interested readers can refer to work documented by Li (2017). There, only the symmetric modes are considered but the procedure to estimate the floater motions is the same. The viscous loads on the floating collar are estimated by the drag term in Morison's equation, as documented in Shen et al. (2018b). Note that in the right-hand side of the motion equations, apart from the viscous forces on the tubes, there are also forces from the net cage and bridle lines. If there is contact and/or connection with the well boat, then there will be also contact and/or connect-line forces from the well boat. The procedure used to estimate such forces is given in section 3.3.

#### *3.2.3. The mooring system*

The set-up of the mooring system is shown in Figure 1. It typically comprises ropes and chains, with buoys to support all mooring lines. Ropes and chains are treated in a similar way as the net and are modeled as elastic trusses with correct diameter, weight and stiffness. The hydrodynamic forces on the mooring lines are estimated by the modified Morison's equation based on the cross-flow principle and by neglecting the longitudinal drag forces. By modified Morison's equation is meant that the local transverse body velocities and accelerations are accounted for.

The complete fish-farm system is solved simultaneously and evolved in a time-stepping procedure that involves solving a linear system of equations for the unknown truss tensions at each time step. Then loads in the mooring lines and in the net cage twines can be obtained.

### *3.3. Contact force estimation*

The well boat is coupled with the fish farm system in two ways: it is connected to the floating collar by two ropes and has also direct contact with the floating collar. For each rope, the connection force is estimated as a linear spring force directed along the connection line and given by the product between the rope spring stiffness and the rope elongation. The latter is easily estimated when the well-boat position and the floating-collar configuration are known. The force is taken as zero if the elongation is negative. The contact force $F_c$ is normal to the surface of the boat when contact with the floating collar happens. Here a simplified method is proposed to deal with the contact between the well boat and the floating collar. Before estimating the contact force, we need to determine whether the contact happens or not. If the distance

between the center line of the floating collar outer tube and the boat surface $\Delta_c$ is smaller than the tube's cross-sectional radius $d_f/2$, then the floating collar gets in contact with the boat. The reason to use the center line is that the motions of the floating collar center line can be readily obtained in the simulations. If the floater gets in contact with the boat, the contact force $F_c$ is assumed to be proportional to $d_f/2-\Delta_c$ and expressed as $F_c = k_c(d_f/2 - \Delta_c)$ with $k_c$ the contact stiffness and $d_f/2 - \Delta_c$ the normal distance between the floating collar outer surface and the boat surface. This means that we model the contact effect like a spring (or multiple springs) with stiffness $k_c$ between the well boat and the floating collar, see Figure 7. The next step is to determine the contact stiffness $k_c$. Ideally, the contact stiffness should be close to infinity to well represent the stiffness of the boat surface, but very small time-step is then needed to guarantee the convergence of the simulations. Practically, we should choose a sufficiently high $k_c$ to ensure correct global response of the coupled system while still reasonable time-steps can be used in the simulations.

For the well boat, the fish farm acts like a spring, preventing the boat from drifting away. The inserted spring stiffness (or contact stiffness) $k_c$ is determined on the basis that the restoring stiffness of the fish farm (with well boat) $k_g$ will not change from its original value (without well boat) $k_f$, namely $k_g = 1/(1/k_c + 1/k_f) \approx k_f$. This means that the inserted spring stiffness $k_c \gg k_f$.

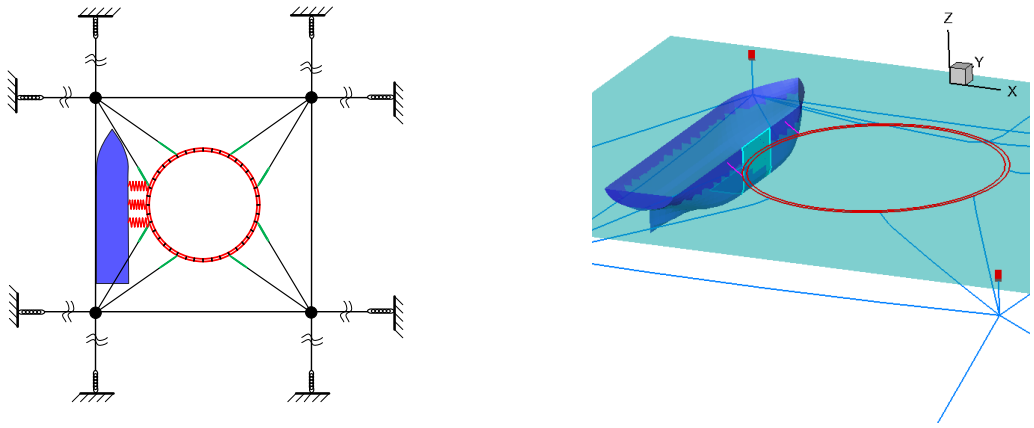


Figure 7: Sketch for explaining the estimation of the well boat-fish farm contact force by very soft springs. Left: bird view. Right: three-dimensional view.

To estimate a suitable value for $k_c$, one must establish a realistic value for $k_f$. Let us assume that the well boat is placed at the fish farm according to set-up A (see Figure 3). Then the equivalent fish-farm stiffness $k_f$ to be compared with $k_c$ can be defined as $k_f = dF_x/dx$. Here $F_x$ is the horizontal force, along the $x_E$-axis, acting at position $\beta = 180^o$ of the floating collar and pointing towards the positive $x_E$-axis while $x$ is the corresponding horizontal displacement along $x_E$-axis. Figure 8 shows the equivalent stiffness $k_f$ of the fish farm without well boat as a function of the pretension force and floating collar stiffness. The figure shows that $k_f$ is not constant when subjected to sufficiently small external force. This is due to the catenary shape of the chains in the lower end of the anchor lines. As the load exerted on the system increases, $k_f$ is almost constant and about 24 kN/m. In this case, there is no anchor chain laying on the seabed and the stiffness of the mooring system is mainly determined by the mooring line stiffness. Larger pretension forces in the anchor lines will increase $k_f$ when small external force is exerted on the system. If we increase the floating collar stiffness, $k_f$ increases, as expected. If we consider a rigid floating collar, then $k_f$ reaches a

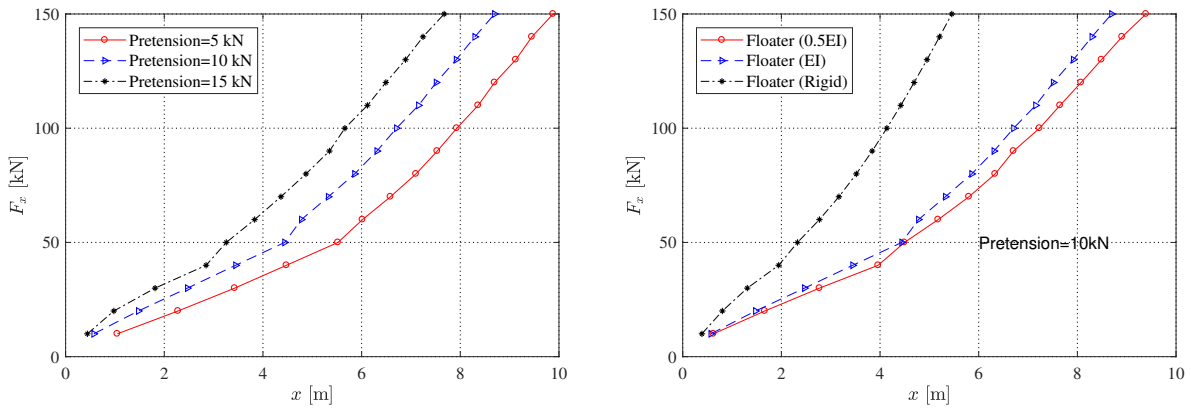


Figure 8: The equivalent stiffness $k_f$ of the fish farm without well boat is represented by the slope of the curve $F_x$. Left: with different pretension forces in the anchor lines. Right: with different floating collar stiffnesses. $EI = 7.27 \times 10^6$ Nm$^2$ is the cross-sectional bending stiffness of the floating collar in the horizontal plane with $E$ the Young's modulus (high-density polyethylene) and $I$ the area moment of the cross-section.

maximum value and the maximum equivalent stiffness $k_{fmax}$ is about 40 kN/m. So it is fairly safe for us to set the contact stiffness between the well boat and the floating collar $k_c = 100k_{fmax} = 4000$ kN/m to ensure correct global restoring stiffness for the well boat.

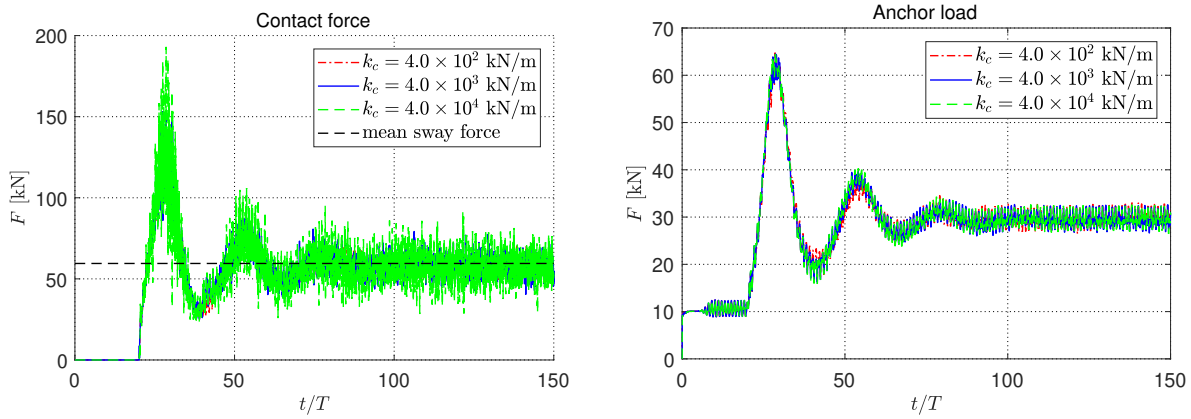


Figure 9: Time histories of the well boat-floating collar contact force (left) and of the loads in anchor line-1 (right) in beam-sea regular waves, i.e. along $x_E$-axis when set-up A is used, with wave period $T = 6$ s and wave height-to-wavelength ratio $H/\lambda = 1/60$. Three different contact stiffnesses $k_c$ are considered.

In order to see how the contact stiffness will influence the mooring forces, time histories of the contact force $F_c$ and the load in anchor line-1 (see Figure 1) with three different values of the contact stiffness, i.e. $k_c = 400$ kN/m, 4000 kN/m and 40000 kN/m, are shown in Figure 9. Regular waves in the $x_E$ direction and set-up A are considered in the analysis. By using regular waves, we can analyze the influence of the contact stiffness on both the mean value and oscillation amplitude of the anchor force. The mean value is relevant for the present study while the oscillation amplitude is imporant for the investigation of the coupled system in irregular waves (Shen et al., 2018a). From the figure, larger high-frequency oscillations are observed when larger contact stiffness is adopted, which is reasonable. However, for the anchor force, relatively small difference is observed for the three examined values of the contact stiffness. This indicates that we can have a reasonable prediction of the global response of the coupled system as long as a reasonably high contact

stiffness is assumed, while locally the contact force may be more sensitive to the contact stiffness. The time histories of the loads in anchor line-1 show that the total anchor load comprises two components: (1) wave frequency component that oscillates with the incident wave period and (2) slowly varying decaying component that oscillates with the natural period $\approx 150$ s of the coupled fish farm-well boat system. The slowly varying resonant oscillation may be excited by nonlinear wave loads when the coupled system is exposed to irregular waves and can significantly increase the mooring loads and floating collar stresses. More discussions for the coupled system in irregular waves can be found in Shen et al. (2018a). In general when contact happens, also a tangential force $F_s$ will act, directed to the opposite direction of the relative tangential velocity between the well boat and the floating collar and estimated as $F_s = \mu F_c$, with $\mu$ the frictional coefficient between the well boat (steel) and the floating collar (high-density polyethylene). According to the experimental results from Dhouibi et al. (2013), the frictional coefficient $\mu$ is in the range $\mu = 0.09 - 0.15$. $\mu = 0.12$ is used in our simulations in the next section.

## 4. Physical investigation of the coupled system in current

In this section, we present a physical investigation of the coupled system in current using the proposed numerical method. The main focus is on how the presence of the well boat will influence the fish farm. Based on the previous description of the proposed numerical model, we expect that the numerical results for the coupled system are reliable. Unfortunately, no experimental data are available for a quantitative validation of our numerical model including the well boat and the fish farm. Performing such model tests is challenging due to the scaling of different components. The coupled system with set-up A (see Figure 3), with the well boat placed at the weather side of the floating collar, is our research focus. Results for the other two set-ups presented in Figure 3 will be considered in selected cases, for comparison. Current with zero incident angle are considered in nominal simulations. "Nominal" denotes that basis values are used in the simulations, for example, for the fish farm, nominal parameters are given in Tables 2 and 3. First, nominal results are shown in section 4.1. Special attention is paid to the load in anchor line-1 (defined in Figure 1) and the floating collar stresses, which are two important parameters for the fish-farm integrity. Then a detailed sensitivity analysis is performed in section 4.2 to identify important parameters affecting the anchor loads and the maximum stress in the floating collar. Finally, the operational conditions of the well boat are discussed and the most important parameters for determining them are proposed in section 4.3.

### *4.1. Nominal results*

Time histories of the loads in anchor line-1 in current are shown in Figure 10. In the simulations, the fish farm is first investigated, then, after about 280 s, the well boat is connected with the fish farm. The considered current velocity varies from 0.1 m/s to 1.0 m/s, covering the scenario from small exposure to high exposure, according to the Norwegian Standard. The figure shows that the mean steady-state anchor loads increase strongly due to the viscous current loads on the well boat. In the right part of the figure, the steady-state anchor loads with and without the well boat are shown. The figure highlights that the anchor load increases by more than 40% in small current velocities and up to 90% in high current velocities due to the well boat. Results for the other two set-ups with boat heading angle $\psi = 270^{\circ}$ and $\psi = 180^{\circ}$ are also

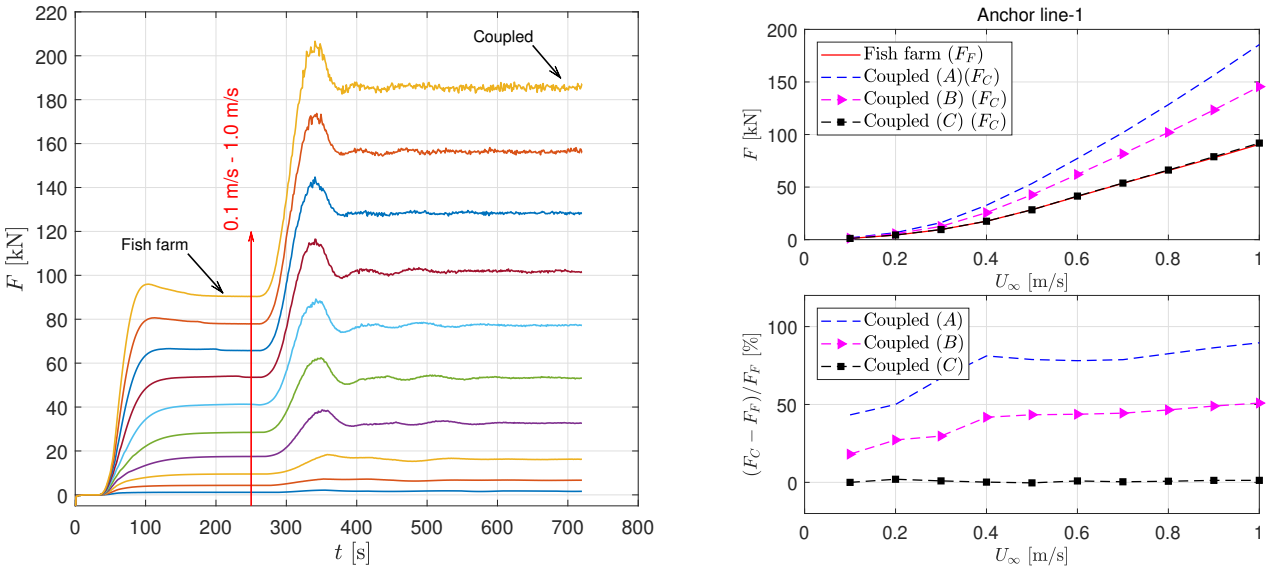


Figure 10: Loads in anchor line-1. Left: time histories of tensions in current. The pre-tension force is subtracted. Current velocity varies from 0.1 m/s to 1.0 m/s. Right: the effect of the well boat on the mean steady-state anchor loads. Results for set-up B and set-up C (see Figure 3) are also provided. $F_F$ and $F_C$ represent the anchor loads for the fish farm only and for the coupled system, respectively.

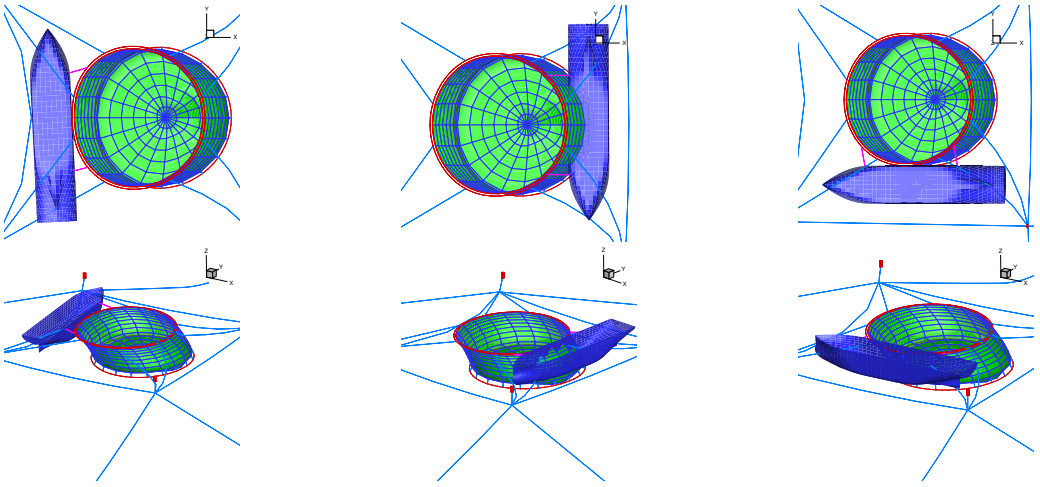

Figure 11: Steady configurations of the coupled system in current. Current velocity $U_\infty = 0.5$ m/s along the $x$-axis. Left: set-up A. Middle: set-up B. Right: set-up C. Upper: bird view. Lower: three-dimensional view.

given. It is not surprising that the well boat has a small influence on the anchor loads for set-up C with boat heading angle $\psi = 180^o$, as the loads on the boat mainly come from the hull friction in this case. The anchor loads for set-up B is about 20% smaller than that for set-up A, this is because the shading effect of the net cage on the ambient flow is considered when estimating the viscous loads on the boat for set-up B. Apart from the flow reduction due to the front part netting, an additional reduction after the flow go through the aft part of the net is also considered for set-up B. Steady shapes of the coupled system with different set-ups are shown in Figure 11.

Figure 12 examines the influence of the well boat on the horizontal deformations of the floating collar. In the left of the figure, time histories of the first seven horizontal mode amplitudes are provided for current velocity $U_\infty$=0.5 m/s. Both the results for the fish farm only and for the coupled system are included.

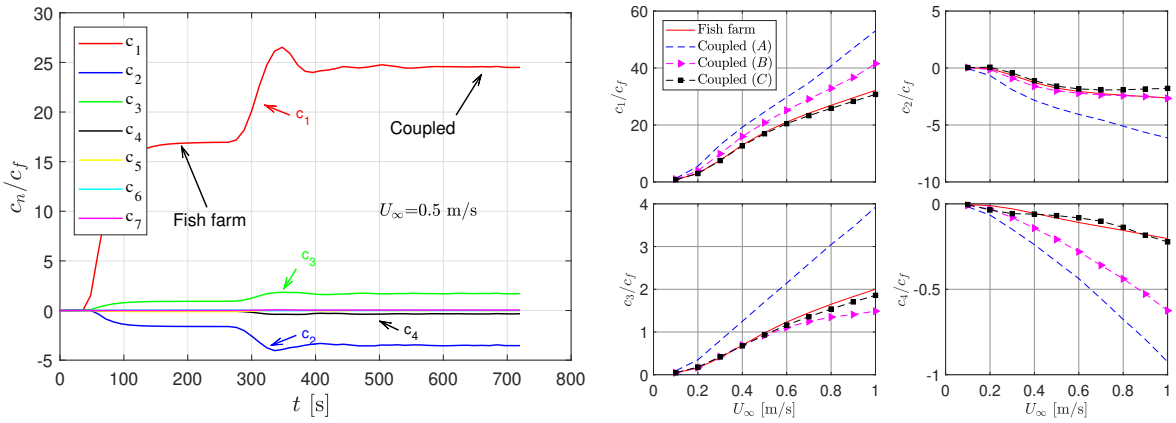


Figure 12: Left: time histories of non-dimensional horizontal floating collar Fourier mode amplitudes $c_n$ in current in set-up A (see Figure 3). Current velocity $U_\infty = 0.5$ m/s. The different mode amplitudes are made non-dimensional by the cross-sectional radius of the floating collar tubes $c_f = d_f/2$. Right: the effect of the well boat on the steady values of surge and first three elastic horizontal mode amplitudes. The results are presented versus current speed. Current velocity varies from 0.1 m/s to 1.0 m/s. Results for cases with set-up B and set-up C are also provided.

From the figure, the first four horizontal modes are the most important and there is a big increase of both rigid-body surge mode ($c_1$) and other elastic modes due to the well boat. The influence of the well boat on the steady values of the first four horizontal mode amplitudes of the floating collar versus current velocity is shown in the right part of the figure. Numerical results indicate that the well boat will strongly increase these mode amplitudes. Considering the current speed $U_\infty$=0.5 m/s, the well boat will increase the first four mode amplitudes by about 41%, 99%, 73.7% and 360%, respectively. Numerical results for the system with set-up B and set-up C are also shown in the figure. Negligible difference is observed in the floating collar deformations with and without the well boat for set-up C. For cases with set-up B, the presence of the well boat will mainly affect the surge motion $c_1$ and the third elastic mode $c_4$. The main reason is that there is no contact between the well boat and the floating collar and the loads from the well boat are transferred to the fish farm through the connection lines.

To see more clearly how the well boat will influence the floating collar, the stress distribution along the floating collar due to horizontal deformations without and with the well boat are shown in Figure 13. The maximum stress due to horizontal deformations at a position $x = R\cos\beta$ along the floating collar is given as

$$\sigma(\beta,t) = \frac{M(\beta,t)}{I} r_{\max} = \frac{E r_{\max}}{R^2} \sum_{n=2}^{\infty} n^2 [c_n(t)\cos n\beta + d_n(t)\sin n\beta] \tag{4}$$

where $r_{\max} = 3c_f$ with $c_f = d_f/2$ the cross-sectional radius of the floating collar, which comprises two tubes, $R = (D_{f1}/2 + D_{f2}/2)/2$ is the mean value of the center line radius of the two tubes. Results are provided for all the three coupling set-ups in Figure 3. From Figure 13, the maximum stress for set-up A occurs at the region where the well boat is in contact with the floating collar while the maximum stress for the two other set-ups occurs at the positions $\beta = 117^o$ and $\beta = 243^o$ where bridle lines are attached. Moreover, the maximum stress for set-up A is much larger than those for the other two set-ups and for the fish farm only. By examining the loads in anchor line-1 and stresses along the floating collar for set-up A and set-up B, we can see that it is more favorable to place the well boat in the leeward side of the fish farm, if one accepts to face higher probability of sucking the net into the well-boat propeller.

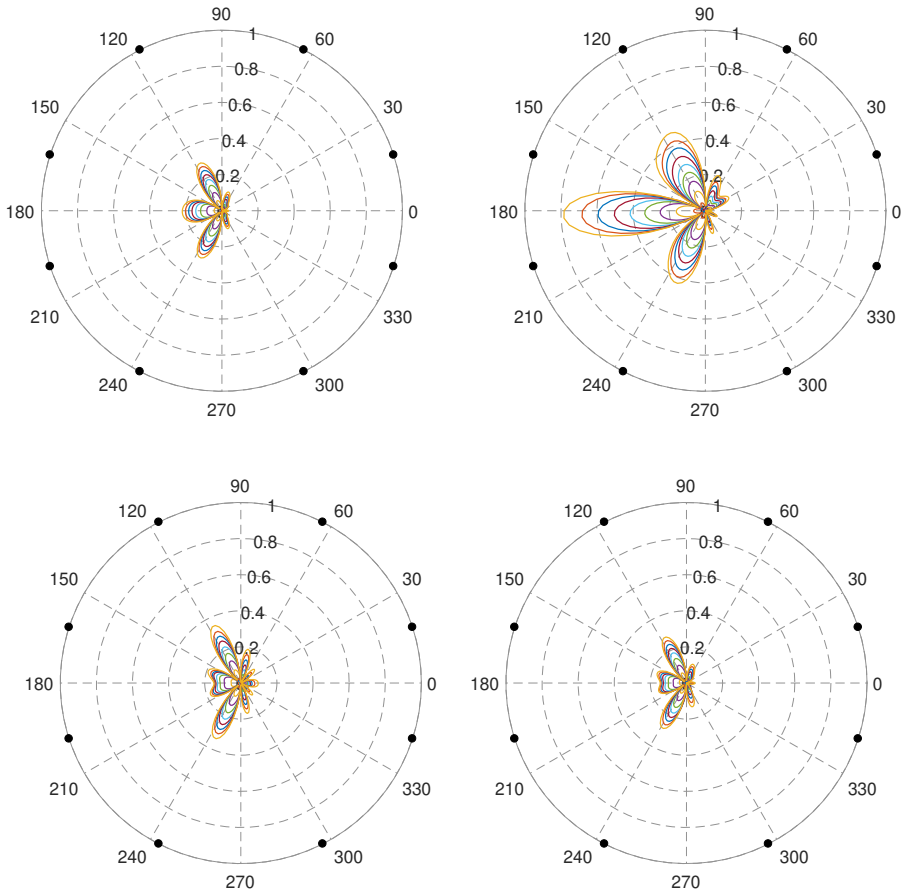


Figure 13: Stress distribution along the floating collar due to horizontal deformations. The stress is made non-dimensional by the yield stress (high-density polyethylene). The labels 0° - 360° represent the radial angle $\beta$ (position) along the floating collar. Upper left: fish farm system only. Upper right: coupled system with set-up A. Lower left: set-up B. Lower right: set-up C. Different lines correspond to different current velocities and from inner to outer they correspond to current velocity $U_\infty$ = 0.1m/s - 1.0m/s. The 8 solid circles in each plot represent the positions where bridle lines are attached to the floating collar.

### *4.2. Sensitivity analysis*

Due to uncertainties in the mathematical modeling and system set-up, we performed a sensitivity analysis for the coupled system in current. The main focus is on the loads in anchor line-1 (defined in Figure 1) and the maximum stresses in the floating collar. As explained before, the well boat is implicitly assumed to be placed at the weather side of the fish farm (set-up A). The different parameters examined are shown in Table 5. In order to quantify the significance of them and try to identify the important ones, we present condensed results in Figure 14. Each bar represents the percentage difference of the load in anchor line-1 (left plot) and the maximum floating collar stress (right plot) with respect to the nominal value, averaged over all the considered current velocities. From the figure, we can see that each parameter has different impact on the examined two parameters. Parameters that lead to more than 5% difference are marked by "$\times$" in the right two columns in Table 5. More detailed discussions are presented in section 4.2.1 for the loads in anchor line-1 and in section 4.2.2 for the maximum stress in the floating collar.

Table 5: Parameters that are varied in the sensitivity analysis for cases in current only. Quantities with subscript 0 mean nominal values, as given in Table 2 and Table 3. Parameters that lead to more than 5% difference from the nominal value of the anchor load and the maximum floating collar stress are marked by "×" in the right two columns. Parameters not investigated are marked by "-".

| | No. | Value | Explanation | >5% | |
|---|---|---|---|---|---|
| | | | | Anchor load | Stress |
| **Environment** | 1 | $\alpha_c = -15^{\circ}$ | Current direction | × | × |
| | 2 | $\alpha_c = 15^{\circ}$ | Current direction | | |
| **Wellboat** | 3 | $C_D = 1.1C_{D0}$ | Drag coefficient | | × |
| | 4 | $C_D = 0.9C_{D0}$ | Drag coefficient | | × |
| **Floating collar** | 5 | $N_h$=1, $N_v$=2 | Rigid body | | - |
| | 6 | $\beta_1 = 90^{\circ}$ and $\beta_2 = 270^{\circ}$ | Boat connection positions | | |
| **Sinker tube** | 7 | $h_s = 0.5h_{s0}$ | Sinker tube depth | × | |
| | 8 | $w_s = 80$kg/m, $W_c = 1000$ kg | Weight in water | × | |
| | 9 | $w_s = 93$kg/m, $W_c = 1500$ kg | Weight in water | × | |
| **Net** | 10 | $U_1 = 1.1U_{\infty}$ | Current velocity (shading effect) | × | |
| | 11 | $U_1 = 1.3U_{\infty}$ | Current velocity (shading effect) | | |
| **Moorings** | 12 | Pretension = 5 kN | Pretension | × | × |
| | 13 | Pretension = 15 kN | Pretension | | × |
| | 14 | $k_s = 2.0k_{s,0}$ | Anchor line stiffness | | |
| | 15 | $m_{\text{chain}} = 0.5\ m_{\text{chain},0}$ | Anchor chain weight | | |
| | 16 | $m_{\text{chain}} = 2.0\ m_{\text{chain},0}$ | Anchor chain weight | × | × |

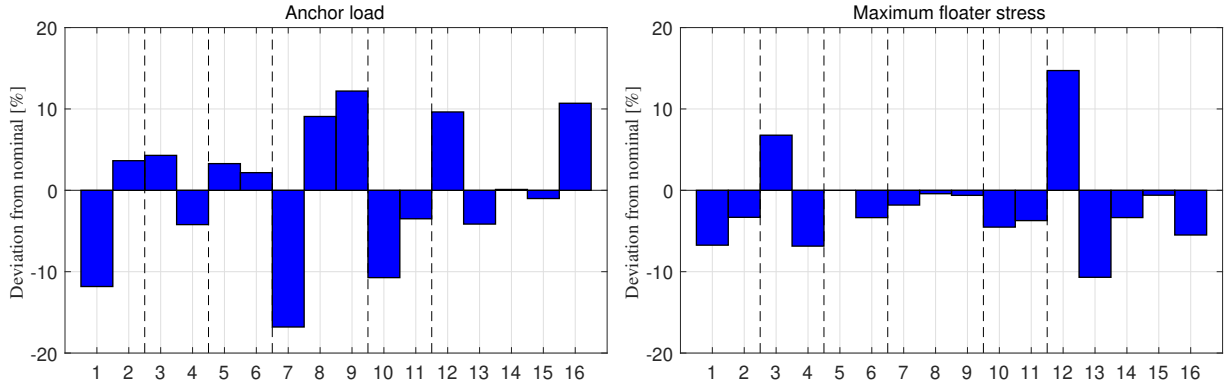


Figure 14: Each bar represents the percentage difference of the anchor load (left) and of the maximum floating collar stress (right) with respect to the nominal value, averaged over all the examined current velocities. The numbers on the horizontal axis refer to the variation number as given in Table 5.

### *4.2.1. Loads in anchor line-1*

*Environment*: In the nominal simulations, zero current direction $\alpha_c = 0^{\circ}$ is assumed. $\alpha_c = -15^{\circ}$ and $\alpha_c = 15^{\circ}$ are considered in the sensitivity analysis to account for the influence of possible change of current direction. Changing the current direction to $\alpha_c = -15^{\circ}$ will reduce the anchor load by about 12%. There are two reasons for the reduction. One is that the current loads on the boat are reduced due to the change of current direction. The other is that the anchor line provides less support to the fish-farm system in the

considered current direction. Small difference is observed with respect to the nominal value for the case with $\alpha_c = 15^o$. This is because smaller load is exerted on the well boat while more load is absorbed by the anchor line, so the joint effects tend to balance each other leading to a small change of the anchor load.

*Well boat*: The cross-sectional drag coefficients $C_D$ for the well boat are estimated empirically, so an error in the boat drag coefficient is expected. Changing the ship averaged drag coefficient by 10% leads to about 4% change of the anchor load with respect to the nominal value.

In the following, we will discuss the influence of the fish farm related parameters on the anchor load.

*Floating collar*: The influence of the floating collar elasticity on the anchor load is studied and numerical results indicate that modeling the floating collar as rigid or as flexible has a small influence on the anchor load. Similar conclusion was drawn in Shen et al. (2018b) for the fish farm without well boat when exposed to current.

In the nominal simulations, the well boat is connected to the floating collar by two ropes at positions $\beta_1 = 135^o$ and $\beta_2 = 225^o$, as shown in Figure 1, while in the sensitivity study $\beta_1 = 90^o$ and $\beta_2 = 270^o$ are examined. Negligible difference is observed when changing the positions where the well boat is connected to the floating collar.

*Sinker tube*: During the loading/offloading operation, the sinker tube may be lifted up for sake of operational convenience and this is not considered in nominal simulations. Lifting the sinker tube up to half of its original depth will reduce the anchor load by 16.8%. To lift the sinker tube, additional 20 ropes between the floating collar and the sinker tube are added, see Figure 15, using similar lift-up configuration as in Nygaard (2013).

A larger weight of the fish-farm bottom is expected to limit the reduction of net-cage volume when the fish farm operates in exposed regions. To investigate quantitatively this effect, two additional bottom weights have been examined and related results are compared with those of the nominal fish-farm set-up. These bottom weights correspond, respectively, to a sinker tube weight $w_s$=80 kg/m with center point weight $W_c$= 1000 kg, and $w_s$=93 kg/m with center point weight $W_c$= 1500 kg. The choices are motivated by expected practical set-ups for fish farms operating in exposed regions. Numerical results show that the anchor load increases by about 9% and 12.2%, respectively, with the two new bottom weights.

*Net cage*: In the nominal simulations, the shading effects of the well boat on the net incoming flow is not considered when evaluating the loads on the net cage. In reality, the presence of the well boat will change the incoming flow and will consequently alter the loads on the net cage. Only the ship wake effect on the front part of the net cage is assessed. To quantify the influence, we need to have a reasonable estimation of the flow distribution behind different sections of the boat. The relative positions of the different well-boat sections to the net cage are shown in Figure 16. The net cage is in the wake of section 3 to section 17. Since we do not have available information on the flow behind each section individually, we divide all the considered sections into two types: with and without bilge keels. For sections with bilge keels (section 7-13), the flow will separate at the leading edge (i.e. at the sharper corner in the weather side) and the flow behind the body is assumed to be similar to that behind a two-dimensional (2D) rectangular body (a block), see the left plot in Figure 17. The center line of the free shear layer $z_m$ is given according to the experimental results from Baker (1977) for the flow behind a 2D block on a wall. Baker (1977) showed that the distribution of

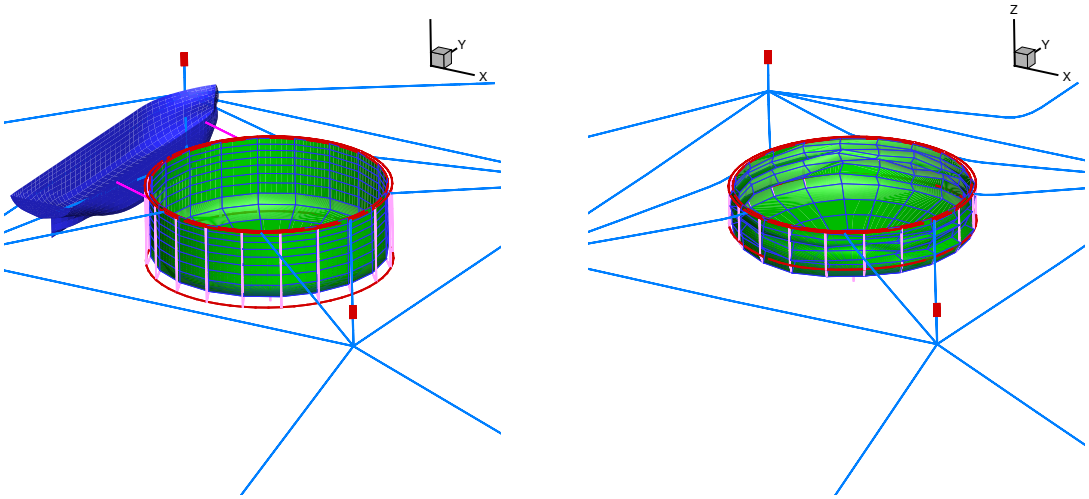


Figure 15: Sketch showing the lifting of the sinker tube up during the loading/offloading operation. Left: initial shape. Right: sinker tube is lifted up (well boat not shown).

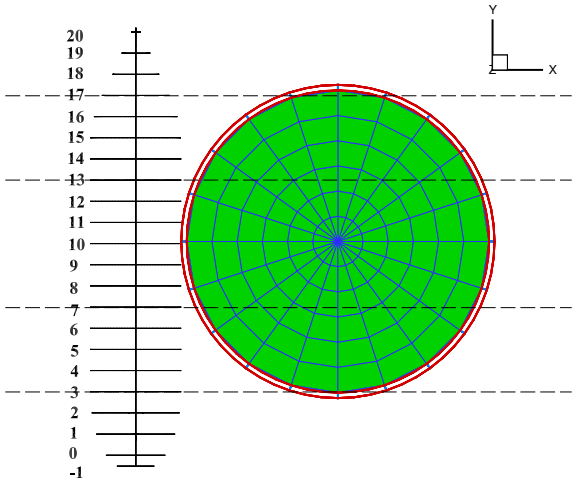


Figure 16: Positions of the different sections of the well boat relative to the net cage from bird view.

mean horizontal velocity in free shear layer behind the 2D block resembles that of a plane mixing layer flow. According to White (2006), the mean velocity profile $\bar{u}$ in a plane mixing layer between parallel streams, with the upper stream moving with mean velocity $U_2$ and the lower stream with mean velocity $U_1$ can be written as

$$\frac{\bar{u}-U_1}{U_2-U_1}=\frac{1}{2}\left[1+\Phi\left(\frac{13.5z}{x}\right)\right] \tag{5}$$

where $\Phi$ is the error function

$$\Phi=\frac{2}{\sqrt{\pi}}\int_0^x e^{-t^2}dt \tag{6}$$

Equation (5) is for the flow with the center line of the free shear layer at $z$=0. For cases with curved shear layer, as in Figure 17, we need to express the formula in a curved coordinate as

$$\frac{\bar{u}-U_1}{U_2-U_1}=\frac{1}{2}\left[1+\Phi\left(13.5\frac{z_s-z_m}{x_s}\right)\right] \tag{7}$$

where $z_m$ is the center line of the shear layer, $x_s$ is a curved coordinate along $z_m$ with $x_s=0$ at the separation point and $z_s$ is a coordinate perpenticular to $x_s$ and pointing upwards. The half thickness of the free shear

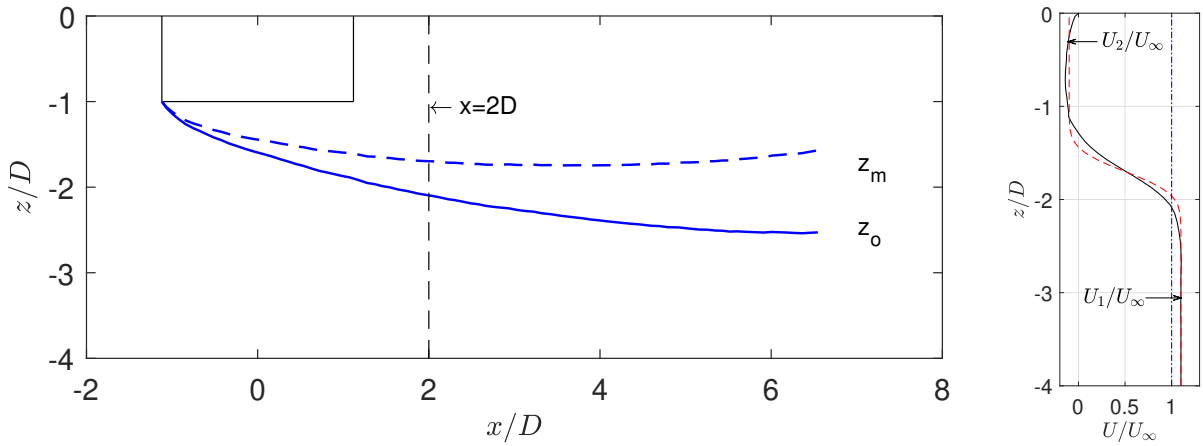


Figure 17: Left: sketch showing important lines for the free shear layer around a section with bilge keels. $z_m$ represents the center line of the free shear layer and $z_0$ the outer boundary of the turbulent separated flow. Both $x$ and $z$ coordinates are made non-dimensional by the draft $D$. Right: distribution of mean horizontal velocity. Solid line: experimental data from Baker (1977). Dashed line: theoretical value for plane mixing layer flow. Dash-dot line: undisturbed inflow velocity.

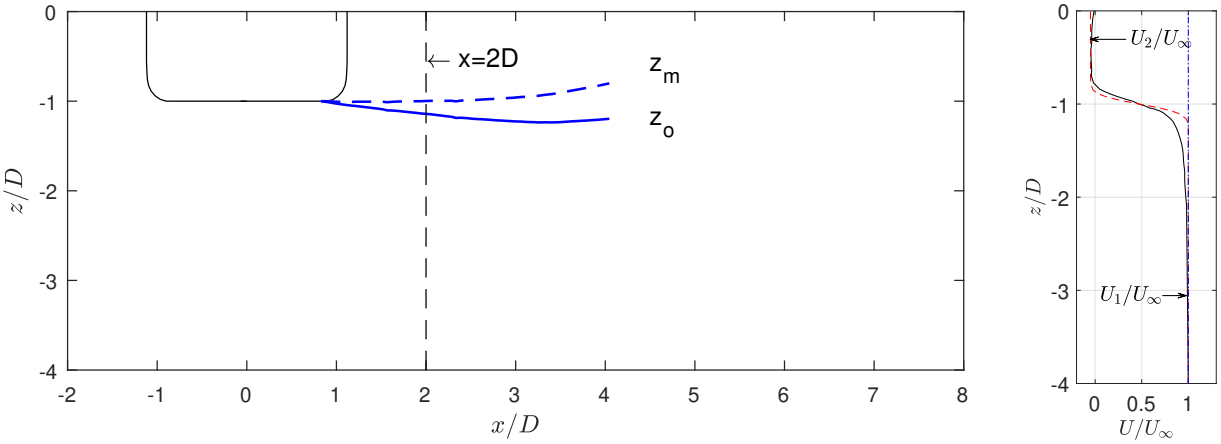


Figure 18: Same as in Figure 17, but for flow around a section without bilge keels.

layer is given by $\tan(7^o)x_s$ (White, 2006), using this, we can identify the outer boundary of the turbulent shear layer $z_o$, as shown in Figure 17. If we can have a reasonable estimation of $U_1$ and $U_2$, then the flow distribution behind these sections can be obtained. In the right plot of Figure 17, a comparison of the mean velocity distribution in free shear layer from the experimental data by Baker (1977) and the theoretical plane mixing layer flow is given. To fit the experimental data, mean lower stream velocity $U_1 = 1.1\ U_\infty$ and and mean upper stream velocity $U_2$ = -0.1 $U_\infty$ are used in the theoretical calculation and good agreement between the experimental and theoretical results is observed. This demonstrates that the plane mixing layer flow can be used to describe the flow behind a 2D block. $U_1 = 1.1\ U_\infty$ means that the flow is accelerated outside the boundary of turbulent flow compared with the incident flow $U_\infty$. $U_2$ = -0.1 $U_\infty$ denotes that there is a small mean reverse flow behind the section.

The obtained free shear layer region is quite similar to the experimental measurements by Chauhan et al. (2017) for the flow past a square prism with a splitter plate attached behind. A difference is the influence of the upstream boundary layer. The Particle Image Velocimetry (PIV) technique is adopted in their measurement. Their experimental results also show that the horizontal velocity is almost constant

outside the turbulent layer with $U_1$ equal to about $1.2U_\infty$ at $x = 2D$ and for $z$ between -4$D$ and -2.2$D$. The main reason for the difference in $U_1$ from the two experiments is that the tests from Chauhan et al. (2017) were performed in water while the tests from Baker (1977) were conducted in air. There exists a very thick boundary layer of the inflow in the front region of the 2D block in Baker (1977), so the inflow mass flux is reduced compared with that in Chauhan et al. (2017). The value of $U_1$ from Chauhan et al. (2017) is believed to be more accurate for our case.

As $U_2$ is small compared with $U_1$, the load on the front upper part of the net cage is expected to have a small contribution to the total net cage load, for simplicity $U_2$ = -0.1$U_\infty$ from Baker (1977) is used in the sensitivity analysis. In terms of $U_1$, two $U_1$ values with $U_1 = 1.1U_\infty$ and $1.3U_\infty$ are investigated. The chosen two $U_1$ values are consistent with the minimum and maximum values of the horizontal velocity at $x = 2D$ with $-4D \leq z \leq -D$, obtained from potential-flow calculation for the section in steady flow. Considering the deformation of the net cage, the velocity profile at position $x = 2D$ is used as the incident flow for the front part of the net cage.

For sections without bilge keels, the flow will separate at the cross-section backward corner in turbulent flow and we assume that the flow behind the body can be described by the flow behind a backward facing step (beam-to-draft ratio $B/D \geq 1$), see Figure 18. The center line of the free shear layer in the figure is given according to the experimental results from Baker (1977). According to Baker (1977), the flow behind a backward facing step can also be seen as a plane mixing layer flow. A comparison of the mean horizontal velocity distribution between experimental data and theoretical results (plane mixing layer flow) is shown in the right plot of Figure 18. $U_1 = U_\infty$ and $U_2 = 0$ m/s are used in the theoretical model. Reasonable agreement is observed. $U_2 = 0$ m/s means that negligible reverse flow is found in the region right behind the cross- section, this is intuitively reasonable because the flow separation is not intense.

The flow is expected to be accelerated below the cross-section with respect to the undisturbed inflow, according to the law of mass conservation. However, the obtained $U_1$ value seems to indicate that this is not the case, see Figure 18. The main reason is that the inflow mass flux is reduced due to a very thick boundary layer of the inflow in the experiments. Larger $U_1$ value should be used for our case. In the sensitivity analysis, $U_2 = 0$ m/s is assumed. For $U_1$, since the flow separates at the backward corner, $U_1$ should be close to the potential-flow solution, from which $U_1$ is between $1.1U_\infty$ and $1.3U_\infty$ at $x = 2D$ with $z$ between -4$D$ and -$D$. This means that we can use the same upper limit and lower limit of $U_1$ both for sections with and for sections without bilge keels. It should be noted that the flow distributions around sections with and without bilge keels can be totally different, even if similar $U_1$ and $U_2$ values are assumed. This is because the length of the free-shear-layer center line $x_s$ is also very important, as shown in eq.(7).

Numerical results show that considering the shading effect of the well boat will reduce the anchor loads by 10.7% with $U_1 = 1.1U_\infty$ and 3.5% with $U_1 = 1.3U_\infty$, respectively. The results denote that the increment of the load on the lower part of the net cage due to the accelerated inflow can not compensate the reduction of the load on the upper part and larger $U_1$ will cause a smaller reduction of the anchor loads.

*Mooring system*: In the nominal simulations, the pretension force in the anchor line is 10 kN, two alternative values of the pretension force are considered in the sensitivity study, i.e. 5 kN and 15 kN, respectively. They correspond to a 50% reduction and a 50% increase of the pretension force, respectively.

Relatively large increase of the anchor loads, about 9.6%, is observed when pretension force equal to 5 kN is adopted. The pretension force is subtracted during the comparison.

Increasing the stiffness of the anchor lines by 100% and reducing the anchor chain weight by 50% has negligible influence on the anchor loads. However, increasing the anchor chain weight by 100% will increase the anchor loads by about 10.5%. This is due to that with larger anchor chain weight, the side anchor lines will have smaller stiffness, so the front two anchor lines need to absorb more loads.

#### *4.2.2. Maximum stress in the floating collar*

From the right plot in Figure 14, the maximum stress in the floating collar is in general sensitive to parameters that are important for estimating the viscous current loads on the well boat. For example, changing the current direction $\alpha_c$ from $0^o$ to $+15^o$ and $-15^o$ will reduce the maximum stress by about 6.7% and 3.3%, respectively, due to the reduction of the current loads on the boat. A variation of the ship averaged drag coefficient by 10 % leads to about 7% change of the maximum stress. The maximum stress is also sensitive to parameters that are closely related with the stiffness of the floating collar, like the pretension force in the anchor line. Larger floating collar stiffness is expected when higher pretension force is applied. Numerical results show that increasing the pretension force in the anchor line from 10 kN to 15 kN will reduce the maximum stress by about 10.7% while reducing the value from 10 kN to 5 kN will increase the maximum stress by about 14.7%. The maximum stress is not so sensitive to parameters associated with the evaluation of the loads on the net cage, like the weight system including sinker tube depth, sinker tube weight and center point weight as well as the shading effect on the incident current field due to the well boat.

### *4.3. Operational conditions*

Operating fish farms in exposed regions will increase the probability of routine well boat operations in severe weather conditions. Nowadays the decision on when performing the operation is mainly dependent on the captain. So it is valuable to have a decision-support tool to give guidance for safe well-boat operations. In this section, we will discuss how to determine the operational conditions of the well boat when the well boat operates at the fish farm during the loading/offloading operation. The well boat is moored at the weather side of the fish farm. The operational conditions are determined based on the criteria that the structural integrity of the fish farm system is not endangered. The loads on the well boat are transferred to the fish farm through direct contact with the floating collar, so the floating collar should be able to withstand the loads. Moreover, the floating collar is moored to the seabed through the mooring system, so the mooring lines should be strong enough. Therefore, two operational criteria are proposed, connected, respectively, with maximum forces in the mooring lines and maximum stress in the floating collar.

In the present paper, we mainly focus on the coupled system in current only. Results of the loads in anchor line-1 and floating collar stresses were shown in Figure 10 and Figure 13. The considered current velocity varies from small exposure to high exposure. The minimum breaking force for the considered anchor polysteel rope is about 628 kN, which is much larger than the maximum force experienced by the anchor line, about 185 kN, so the anchor load is not the main concern when determining the operational conditions. The loads in the two bridle lines are also examined, the maximum loads are slightly smaller than that in anchor line-1 and will also not exceed the breaking limit for the considered sea states. The maximum stress

in the floating collar occurs in the region where the well boat is in contact with the floating collar with a value about 80% of the yield stress for the considered current velocities. Although the maximum stress does not exceed the yield stress in the present study, the results indicate that this response variable is of concern in current and it is expected to be even more critical in combined waves and current.

## 5. Conclusions

A numerical study of a coupled system with a well boat operating at the fish farm in current was performed. The main target was to quantify the influence of the well boat on the fish farm and to determine the operational conditions of the well boat. A modern design well boat and a realistic fish farm were considered in the analysis. The fish farm (with single cage) comprises a floating collar with two concentric tubes, an elastic sinker tube, a flexible-closed net cage and a complex mooring system. The viscous cross-flow loads on the well boat without the net cage and mooring loads on the net cage without the well boat are numerically predicted with experimentally validated methods. However, there is a need for model tests with the coupled system.

Detailed analysis of the load in one of the front anchor lines and of the floating collar motions was performed when the well boat was moored at the weather side of the fish farm. The current transverse viscous loads on the boat were estimated by the cross-flow principle and the cross-sectional drag coefficients were estimated empirically. Numerical results showed that the anchor load increases significantly due to the viscous forces on the boat. A big increase of the floating collar horizontal deformations (both rigid and elastic modes) was also observed and the maximum stress due to the horizontal deformations occurs at the region where the well boat is in contact with the floating collar.

Due to uncertainties in mathematical modeling and system parameters, a systematic sensitivity analysis was performed, to identify the dominant factors when modeling the coupled system. The main focus was on the load in anchor line-1 and the maximum stress in the floating collar. In order to have a more reliable prediction of the anchor load, we should know more accurate values of the environment related parameters (current direction); the fish-farm related parameters (weight system including sinker tube depth, sinker tube weight and center point weight) and the mooring system properties (pretension load, anchor chain weight). In particular, lifting the sinker tube up to half of its original depth would lead to a significant reduction of the anchor load, by about 16.8%. Accurate estimation of the cross-sectional drag coefficients for the well boat and of the shading effect on the current field due to the well boat are not straightforward. However the sensitivity analysis showed that they have moderate effect on the anchor loads. In terms of the maximum floating collar stress, it is more sensitive to well-boat loads related parameters (current direction, cross-sectional drag coefficient) and pretension load in the anchor lines; less sensitive to parameters associated with the loads on the net cage (sinker tube depth, sinker tube weight, etc).

Lastly, the operational conditions of the well boat when it operates at the fish farm were investigated. Two criteria were chosen: maximum loads in the mooring lines and maximum stresses in the floating collar. Numerical results showed that the mooring system could withstand the loads transferred from the well boat for the considered current velocities. The maximum stresses in the floating collar reached values close to the yield stress for the examined maximum current velocity and should be a major concern.

**Acknowledgement**

This work was supported by the Research Council of Norway through the Centers of Excellence funding scheme AMOS, project number 223254. Rolls-Royce Marine is acknowledged for providing the geometry information of the well boat.

**References**

Aarsnes, J. V., Faltinsen, O. M., Pettersen, B., 1985. Application of a vortex tracking method to current forces on ships. In: Proceedings of Proc. Conf. Separated Flow around Marine Structures, Trondheim. pp. 309–346.

Baker, S., 1977. Regions of recirculating flow associated with two-dimensional steps. Ph.D. thesis, University of Surrey.

Bardestani, M., Faltinsen, O. M., 2013. A two-dimensional approximation of a floating fish farm in waves and current with the effect of snap loads. In: ASME 2013 32nd International Conference on Ocean, Offshore and Arctic Engineering. American Society of Mechanical Engineers, pp. V009T12A020–V009T12A020.

Blevins, R. D., 1984. Applied Fluid Dynamics Handbook. New York, Van Nostrand Reinhold Co.

Chauhan, M. K., More, B. S., Dutta, S., Gandhi, B. K., 2017. Effect of attached type splitter plate length over a square prism in subcritical reynolds number. In: Fluid Mechanics and Fluid Power–Contemporary Research. Springer, pp. 1283–1292.

Cummins, W., 1962. The impulse response function and ship motions. Schiffstechnik 9, 101–109.

Delany, N. K., 1953. Low-speed drag of cylinders of various shapes. NACA Tech. Note 3038.

Dhouibi, S., Boujelbene, M., Kharrat, M., Dammak, M., Maalej, A., 2013. Friction behavior of high density polyethylene (hdpe) against 304l steel: An experimental investigation of the effects of sliding direction, sliding history and sliding speed. Journal of Surfaces and Interfaces of Materials 1 (1), 71–76.

Dong, G.-H., Hao, S.-H., Zhao, Y.-P., Zong, Z., Gui, F.-K., 2010a. Elastic responses of a flotation ring in water waves. Journal of Fluids and Structures 26 (1), 176–192.

Dong, G.-H., Xu, T.-J., Zhao, Y.-P., Li, Y.-C., Gui, F.-K., 2010b. Numerical simulation of hydrodynamic behavior of gravity cage in irregular waves. Aquacultural Engineering 42 (2), 90–101.

Faltinsen, O. M., 1990. Sea Loads on Ships and Ocean Structures. Cambridge University Press.

Faltinsen, O. M., 2005. Hydrodynamics of High-speed Marine Vehicles. Cambridge University Press.

Faltinsen, O. M., Kjaerland, O., Liapis, N., Walderhaug, H., 1979. Hydrodynamic analysis of tankers at single point mooring systems. In: Proceedings of the 2nd International Conference Behaviour of Offshore Structures. Vol. 2. pp. 177–206.

Faltinsen, O. M., Shen, Y.-G., 2018. Wave and current effects on floating fish farms. Journal of Marine Science and Application, accepted.

He, Z., Faltinsen, O. M., Fredheim, A., Kristiansen, T., 2015. The influence of fish on the mooring loads of a floating fish farm. In: Proceedings 7th International Conference on Hydroelasticity in Marine Technology. Split, Croatia.

Huang, C.-C., Tang, H.-J., Liu, J.-Y., 2006. Dynamical analysis of net cage structures for marine aquaculture: Numerical simulation and model testing. Aquacultural Engineering 35 (3), 258–270.

Huang, C.-C., Tang, H.-J., Liu, J.-Y., 2008. Effects of waves and currents on gravity-type cages in the open sea. Aquacultural Engineering 38 (2), 105–116.

Kristiansen, T., Faltinsen, O. M., 2012. Modelling of current loads on aquaculture net cages. Journal of Fluids and Structures 34, 218–235.

Kristiansen, T., Faltinsen, O. M., 2015. Experimental and numerical study of an aquaculture net cage with floater in waves and current. Journal of Fluids and Structures 54, 1–26.

Lader, P., Jensen, A., Sveen, J. K., Fredheim, A., Enerhaug, B., Fredriksson, D., 2007. Experimental investigation of wave forces on net structures. Applied Ocean Research 29 (3), 112–127.

Lader, P. F., Fredheim, A., 2006. Dynamic properties of a flexible net sheet in waves and current: A numerical approach. Aquacultural Engineering 35 (3), 228–238.

Li, L., Fu, S., Xu, Y., 2013. Nonlinear hydroelastic analysis of an aquaculture fish cage in irregular waves. Marine Structures 34, 56–73.

Li, P., 2017. A theoretical and experimental study of wave-induced hydroelastic response of a circular floating collar. Ph.D. thesis, Norwegian University of Science and Technology.

Li, P., Faltinsen, O. M., Lugni, C., 2016. Nonlinear vertical accelerations of a floating torus in regular waves. Journal of Fluids and Structures 66, 589–608.

Løland, G., 1991. Current forces on and flow through fish farms. Ph.D. thesis, Norwegian University of Science and Technology.

Marichal, D., 2003. Cod-end numerical study. In: Third International Conference on Hydroelasticity in Marine Technology. Oxford, UK.

Mercier, R. S., Huijs, F. A., 2005. Steady Current Forces On Tanker-based FPSOs. Vol. 84. WIT Press.

Nakaguchi, H., Hashimoto, K., Muto, S., 1968. An experimental study on aerodynamic drag of rectangular cylinders. The Journal of the Japan Society of Aeronautical Engineering 16 (168), 1–5.

NS9415, 2009. Marine fish farms - requirements for site survey risk, analysis, design, dimensioning, production,installation and operation. Norwegian standard.

Nygaard, I., 2013. Merdforsøk. kapasitets-tester. interaksjon mellom not og utspilingssystem. Tech. rep., Tech. rep., Norsk Marinteknisk Forskningsinstitutt AS.

Shen, Y.-G., Greco, M., Faltinsen, O. M., 2016. Wave-induced vertical response of an elastic circular collar of a floating fish farm. In: The 12th International Conference on Hydrodynamics (ICHD 2016). Egmond aan Zee, Netherlands.

Shen, Y.-G., Greco, M., Faltinsen, O. M., 2018a. Numerical study of a well boat operating at a fish farm in long-crested irregular waves and current. Journal of Fluids and Structures, submitted.

Shen, Y.-G., Greco, M., Faltinsen, O. M., Nygaard, I., 2018b. Numerical and experimental investigations on mooring loads of a marine fish farm in waves and current. Journal of Fluids and Structures 79, 115–136.

White, F. M., 2006. Viscous Fluid Flow. Vol. 3. McGraw-Hill New York.

Xu, T.-J., Dong, G.-H., Zhao, Y.-P., Li, Y.-C., Gui, F.-K., 2011. Analysis of hydrodynamic behaviors of gravity net cage in irregular waves. Ocean Engineering 38 (13), 1545–1554.

Xu, T.-J., Zhao, Y.-P., Dong, G.-H., Li, Y.-C., Gui, F.-K., 2013. Analysis of hydrodynamic behaviors of multiple net cages in combined wave–current flow. Journal of Fluids and Structures 39, 222–236.

Zhan, J., Jia, X., Li, Y., Sun, M., Guo, G., Hu, Y., 2006. Analytical and experimental investigation of drag on nets of fish cages. Aquacultural Engineering 35 (1), 91–101.

Zhao, Y.-P., Li, Y.-C., Dong, G.-H., Gui, F.-K., Teng, B., 2007. A numerical study on dynamic properties of the gravity cage in combined wave-current flow. Ocean Engineering 34 (17), 2350–2363.